Journal of Sustainable Cement-Based Materials

ISSN: 2165-0373 (Print) 2165-0381 (Online) Journal homepage: www.tandfonline.com/journals/tscm20

Properties of limestone calcined clay cement (LC3) mortar under different types of biochar – hydration kinetics, strength development, and chloride resistance

Xuqun Lin, Quang Dieu Nguyen, Arnaud Castel, Zhizhong Deng, Yu Pang, Yuxuan Yang & Vivian W.Y. Tam

To cite this article: Xuqun Lin, Quang Dieu Nguyen, Arnaud Castel, Zhizhong Deng, Yu Pang, Yuxuan Yang & Vivian W.Y. Tam (28 Mar 2026): Properties of limestone calcined clay cement (LC3) mortar under different types of biochar – hydration kinetics, strength development, and chloride resistance, Journal of Sustainable Cement-Based Materials, DOI: 10.1080/21650373.2026.2649525

To link to this article: https://doi.org/10.1080/21650373.2026.2649525

Published online: 28 Mar 2026.

Journal of Sustainable Cement-Based Materials, 2026
http://dx.doi.org/10.1080/21650373.2026.2649525

Properties of limestone calcined clay cement (LC3) mortar under different types of biochar – hydration kinetics, strength development, and chloride resistance

Xuqun Lin[a], Quang Dieu Nguyen[a]*, Arnaud Castel[a]*, Zhizhong Deng[a], Yu Pang[a], Yuxuan Yang[a] and Vivian W.Y. Tam[b]

[a]*School of Civil and Environmental Engineering, University of Technology Sydney, Ultimo, NSW, Australia;* [b]*School of Engineering, Design of Built Environments, Westen Sydney University, Sydney, NSW, Australia*

(Received 30 October 2025; Accepted 18 March 2026)

Biochar has been emerging as a new cement-replacement solution for sustainable concrete developments. This study compared the performances of three different types of biochar, including hydration process, strength development, and chloride resistance. Samples with 5 wt% wheat straw biochar (WSB) promoted the cement hydration heat by 3.34% when compared to the control group, leading to slight compressive and flexural strength improvements at 28 days. High mass of bound water and portlandite in thermogravimetric analysis results supported the favorable benefit of WSB to promote the cement hydration. Finer-size WSB also reduced passing charge in rapid chloride penetration test and penetration depth in chloride migration test. WSB5 group had the highest electrical resistivity among all samples using Nyquist Plot. Finally, our study recommended that up to 10 wt% fine-size wheat straw biochar (size $\leq$ 70 µm) could be conservatively used to replace cement for sustainable concrete design.

Keywords: Biochar; LC3; hydration; durability; microstructure

1. Introduction

Concrete has been widely used for many modern structures, from residential buildings to large infrastructures, due to its durable and economic aspects. Although concrete provides a proper solution for structural application designs, the production of cement accounts for approximately 6-7% of the total CO_2 emissions in the globe [1]. Meanwhile, based on the study by Imbabi et al. [2], this trend was expected to increase as the cement production may be quadrupled by 2050. As a result, appropriate alternatives are urgently required to reduce the cement usage while maintaining mechanical and durability properties of the cementitious composites.

Numerous studies [3–5] suggested that one of the most effective ways to lower the carbon footprint of the concrete structures was to partially replace cement content using industrial by-products, including waste glass powder (WGP) [6,7], steel slag [8,9], and fly ash (FA) [10,11]. According to Pan et al. [12], the addition of 20–40 wt% WGP lowered the early-age hydration of the WGP-cement composites due to the dilution effect of cement, leading to lower compressive strength (−9.6% to −12.1%) than WGP-free samples at 28 days. Li et al. [13] observed that the compressive strength of sample with 20 wt% waste glass powder (size of 44–74 µm) was improved by 15.6% when compared to that of WGP-free specimens at 28 days. They also reported that finer-size WGP (size $\leq$ 44 µm) led to better compressive strength development, due to its relatively high reactivity promoting the cement hydration. Zhao et al. [14] reported that replacing cement using 20 wt% steel slag (namely CFCS group) led to a 33.6% compressive strength increase when compared to the reference group at 28 days. They also observed that CFCS group had accelerated hydration kinetics and lower setting time than the control group. In the RCPT test by Pan et al. [15], using 10 wt% steel slag to replace cement promoted 17.32% reduction on the passing coulomb when compared to the control group at 28 days. Li et al. [16] found that although the addition of 10 to 30 wt% fly ash replacing cement led to 15.5% to 26.8% 7-day compressive strength reduction, the presence of fly ash refined the pore structures of the FA-cement composites for a denser microstructure. However, although those supplementary cementitious materials (SCMs) are favorable alternatives lowering the cement usage for sustainable concrete, there will be limitations for many countries and regions without direct supply of those by-products, since the SCMs transportation would be a major concern contributing to relatively high cost and additional carbon footprint. As a result, it is highly demanding to explore new alternatives to partially replace cement using local resources with high availability.

Biochar, originated from the oxygen-limited pyrolysis production based on different biomass, have been emerging as a new cement-replacement solution for sustainable cementitious composites [17–19]. Kalderis et al. [20] observed that the samples with 2 wt% olive tree biochar had reduced porosity by 27.79% and capillary adsorption by 27.34% when compared to the control group at 28 days. Ye et al. [21] found that 2 wt% corn stover biochar

*Corresponding author. Emails: quangdieu.nguyen@uts.edu.au; arnaud.castel@uts.edu.au

addition promoted the cement hydration and filled in pores of the cementitious matrix, leading to a denser microstructure. Gupta et al. [22] found that replacing cement using 1– 2 wt% rice husk biochar reduced NaCl solution permeability into the biochar-cement composites. Furthermore, Lin et al. [23] reported that using up to 5 wt% waste wood biochar to replace cement slightly promoted the 28-day compressive strength by 6.5% when compared to biochar-free samples. They also observed that the presence of pulverized biochar led to a denser microstructure resisting the ingress of chloride and sulfate ions. Kua et al. [24] reported that the presence of rice husk biochar led to a reduced permeability of biochar-LC3 composites, while increasing the carbon dioxide capture and mineralization. Furthermore, several studies [25–27] also observed that due to filler effect and internal curing, biochar addition promoted the strength development of the biochar-LC3 composites. Although aforementioned studies have reported the advantage of biochar (cement replacement up to 5 wt%) in improving chloride resistance of the biochar-cement composites, there are limited studies analyzing the effects of different biochar on the resistance of chloride-ion penetrations of the cementitious composites with up to 10 wt% biochar as cement replacement. Thus, it is worthy assessing how different biochar affects the strength development and chloride-resistance performances of the biochar cement composites with different replacement percentages. Another significance of this study is to consider LC3 as the binder of the biochar composite.

In this study, three different biochar were utilized to investigate potential effects on the properties of the biochar-cement mortars, including waste wood biochar (WB), bamboo biochar (BB), and wheat straw biochar (WSB). This study compared their influences on hydration kinetics and strength development of the cementitious composites up to 28 days. Rapid Chloride Penetration Test (RCPT) and Chloride Migration Test (CMT) were designed to access the chloride resistances of samples with different biochar. Furthermore, bulk resistivity test was used to compare the electrical conductivity of various biochar-cementitious composites. The microstructural analyses were conducted using Scanned Electron Microscopy equipped with Energy dispersive X-ray spectroscopy (SEM-EDS), X-ray diffraction (XRD), and Thermogravimetric analysis (TG).

2. Methodology

2.1. Raw materials and specimen preparations

Cementitious mortars were fabricated using General purpose cement (GPC) from Boral Australia. Two locally available biochar, including waste wood biochar (WB) and wheat straw biochar (WSB), were obtained from Rainbow Bee Eater Biochar (Australia). These two biochar were produced based on pyrolysis at temperature of 500 °C for one hour. Bamboo biochar (BB) was purchased from Shengxiang Biochar Company (Gongyi City, China). BB was produced using the process as for the other two biochar (WB and WSB). Three biochar were then ground into powder using a ring mill for 30 s (Figure 1). It is worth noting that limestone powder (Boral, Australia) and calcined clay (Argeco, France) were used to reduce the cement usage (Figure 1g–1h), further improving the sustainability of the biochar-cement composites. As shown in Figure 1, biochar has porous microstructure with different shapes. WB has thick wall with round pores (Figure 1b), and round-shape pores with various sizes randomly distribute in BB particle (Figure 1f). However, the SEM image of WSB (Figure 1d) depicts a totally different morphology with thicker wall, where small amount of eclipse-shape pores is observed. Figure 2 depicts the particle size distribution of different powders using a Malvern 2000 Particle Size Analyzer. It should be noted that, based on 15–20 min ultrasonic rotation, a good powder dispersion in distilled water could be observed. It could be noted that WSB had relatively finer particle size (up to 70 μm) than other two biochar with D50 value of 13.18 μm and D90 value of 30.19 μm. WB had relatively larger particle size (up to 239.88 μm) with D50 value of 19.95 μm and D90 value of 79.43 μm. The chemical compositions of different binders were shown in Table 1. All three biochar had relatively high content of SiO_2, followed by Al_2O_3, and CaO.

The mix designs of all groups were listed in Table 2. The water to binder ratio and sand to binder ratio was set as 0.5 and 2.5 respectively. The mortar fabrications with different dimensions were summarized in Table 3. This study adopted LC3 formulation of 20 wt% calcined clay and 10 wt% limestone, as per a previous study [28]. CLC was the reference group with 20 wt% calcined clay and 10 wt% limestone as cement replacement. In terms of biochar application, two replacement percentage were designed, including 5 wt% (namely BB5, WB5 and WSB5) and 10 wt% biochar (namely BB10, WB10, and WSB10). Thus, the effects of different biochar with various replacement percentages on the properties of the biochar-cement composites could be compared.

Initially, all powders were dry mixed using a 10 L Hobar Mixer at speed of 16 rpm for 2 mins, aiming a uniform powder mixture. Then, a mixing speed of 24 rpm was applied for 4 mins after adding ½ water content. Another 3 min mixing was set at 24-rpm speed after adding the rest water content. Superplasticiser (Sikament® Eco WR, Sika Australia) was added during the mixing achieving comparable flows for specimens with and without biochar (Table 1). After that, fresh cementitious mixture was poured into corresponding molds as mentioned in Table 2. All molds were then placed on the vibration table followed by a 2-min vibration for a uniform compaction. It should be noted that all molds were covered using plastic foil till the 24-hour demoulding. Finally, all samples were marked and placed in a water tank until testing.

2.2. Hydration kinetics by isothermal calorimetry

It should be noted that additional cementitious pastes were prepared for each group based on Table 1. 10 g of fresh pastes were collected from each group and placed in a calorimeter container. A TAM air isothermal calorimetry was used to measure the corresponding heat development of the cement hydration. The temperature was set at 20 °C

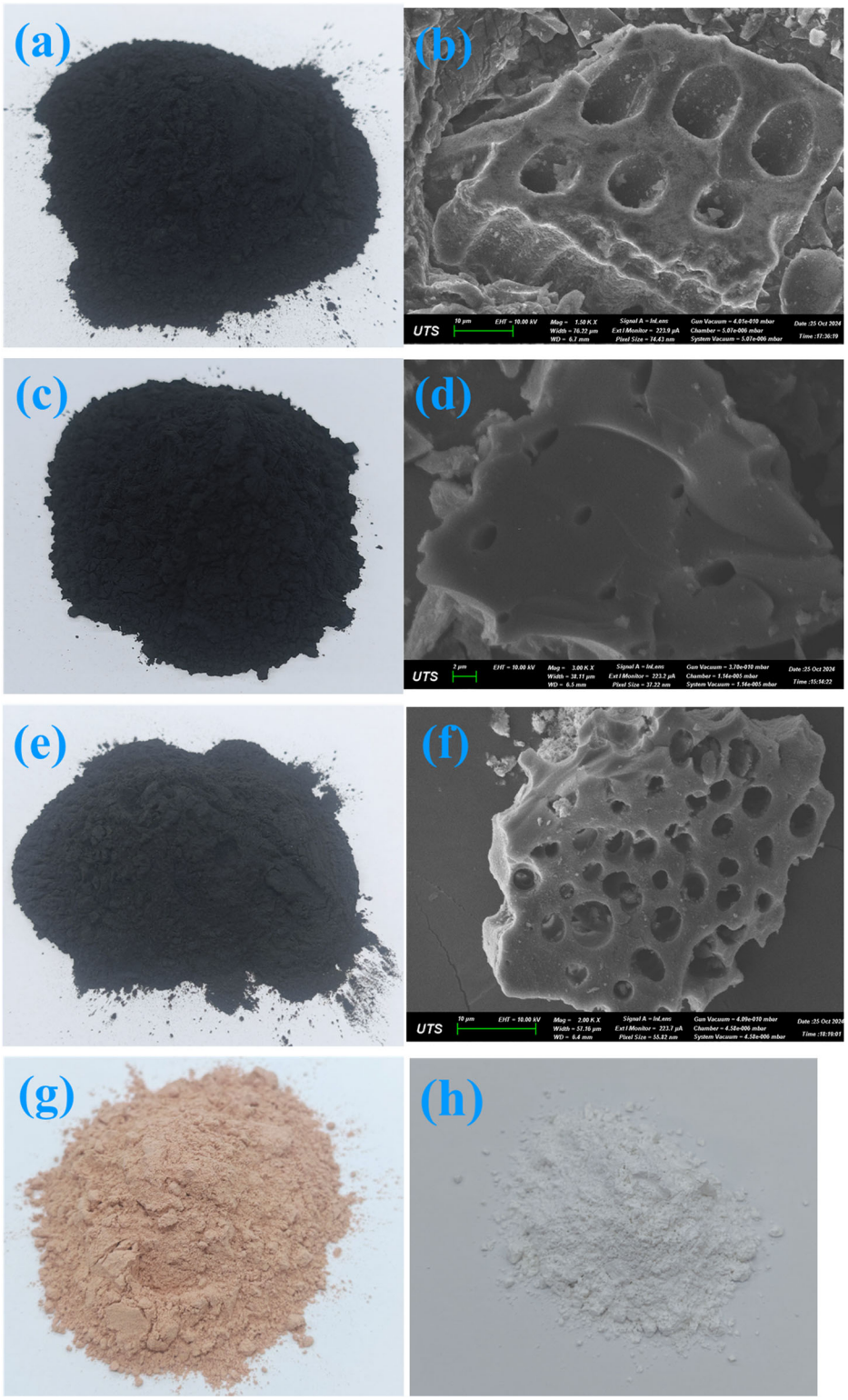

Figure 1. Morphologies of raw materials: (a) waste wood biochar (WB); (b) SEM image of WB; (c) wheat straw biochar (WSB); (d) SEM image of WSB; (e) bamboo biochar (BB); (f) SEM image of BB; (g) calcined clay; (h) limestone.

and the hydration progress remained up to 72 h. Finally, the data of heat evolution was collected and analyzed for each group.

2.3. Mechanical properties testing

Cementitious cubes and prisms were immersed in a water tank before 7-day and 28-day testings. As per ASTM C348-21[29], flexural strength testings were performed at 7 days and 28 days of exposure using a AGX 50 universal testing machine. Complying with ASTM C109-20 [30], a UH500 universal testing machine was used to test 7-day and 28-day compressive strength. It should be noted that 3 samples in each group were tested accordingly, and 7-day and 28-day mechanical properties of each group were the average value of three identical results.

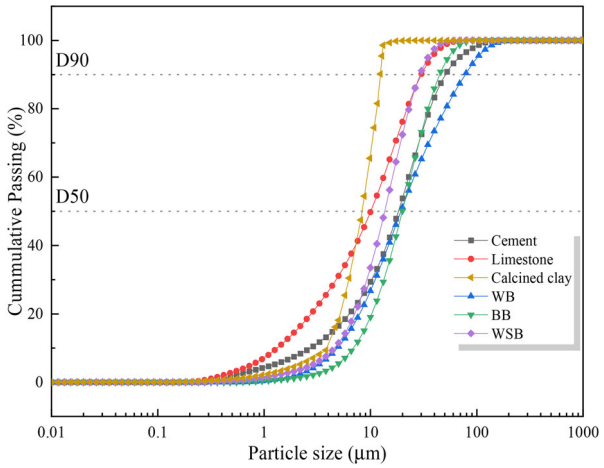

Figure 2. Particle size distribution of powders.

samples were dried at a temperature of 50 °C for a week and ground into powders passing a 200-μm sieve. Samples for SEM-EDS analysis were cast in epoxy resin (Wizbe Industries Clear Epoxy Resin) followed by a polishing process using a Struers Tegramin-30 polisher as per literatures [31,32]. Finally, polished samples were stored in an oven with a temperature of 40 °C till the formal testing. A Zeiss Supra 55VP Scanning Electron Microscopy (SEM) with energy dispersive X-ray spectroscopy (EDS) was used to analyze the morphologies of hydration products in different cementitious matrix. Polished samples were coated with 12 nm chromium using a Quorum Q150V coater. The SEM-EDS was operated with a working distance of 4.5-8 mm at voltage of 10 kV.

A NETZSCH STA 449 Jupiter was used to determine

Table 1. XRF results of raw materials.

Chemical compositions	Cement	Calcined clay	limestone	WSB	BB	WB
CaO	63.73	0.81	57.56	11.51	3.54	19.15
Al_2O_3	5.14	21.36	0.13	8.74	9.45	3.95
SiO_2	18.94	70.34	0.34	62.15	74.15	57.62
P_2O_5	0.20	0.01	–	3.52	–	2.29
SO_3	2.49	0.32	–	2.14	3.64	1.33
Na_2O	0.25	0.12	–	2.13	0.13	5.15
MgO	1.48	0.17	0.28	4.31	0.15	3.15
K_2O	0.47	0.21	–	2.36	3.41	1.58
TiO_2	0.29	1.10	–	0.11	–	0.12
V_2O_5	0.02	0.01	–	0.02	0.03	0.03
Fe_2O_3	3.00	2.56	0.1	2.03	3.68	1.67
L.O.I.	3.989	2.993	41.59	0.98	1.82	3.96

Table 2. Mix designs for strength and durability testings.

Mix designs	GPC	CC	LS	Water	Sand	BB	WSB	RHB	Super-plasticiser	Flow (mm)
CLC	0.7	0.2	0.1	0.5	2.5	–	–	–	–	201 ± 2.1
BB5	0.65	0.2	0.1	0.5	2.5	0.05	–	–	0.005	203 ± 1.4
BB10	0.6	0.2	0.1	0.5	2.5	0.1	–	–	0.01	199 ± 2.5
WB5	0.65	0.2	0.1	0.5	2.5	–	0.05	–	0.005	200 ± 1.7
WB10	0.6	0.2	0.1	0.5	2.5	–	0.1	–	0.01	198 ± 3.4
WSB5	0.65	0.2	0.1	0.5	2.5	–	–	0.05	0.005	202 ± 1.2
WSB10	0.6	0.2	0.1	0.5	2.5	–	–	0.1	0.01	200 ± 2.7

Note: CLC donates the control group, CC refers to calcined clay, LS is limestone, BB5 means samples with 5 wt% BB to replace cement, BB10 is samples with 10 wt % BB to replace cement, WB5 refers to samples with 5 wt% WB to replace cement, WB10 is samples with 10 wt % WB to replace cement, WSB5 means samples with 5 wt% WSB to replace cement, and WSB10 is samples with 10 wt % BB to replace cement.

Table 3. Sample casting programme.

Experimental method	Specimens	Mould dimensions	Exposure condition
7-day and 28-day compressive strength	3,3	$50mm \times 50mm \times 50mm$	7-day/28-day curing in water tank
7-day and 28-day flexural strength	3,3	$40mm \times 40mm \times 160mm$	7-day/28-day curing in water tank
Bulk resistivity	3	$40mm \times 40mm \times 160mm$	28-day curing in water tank
Rapid chloride penetration test (RCPT)	3	$\emptyset 100mm \times 200mm$	28-day curing in water tank
Chloride migration test (CMT)	3	$\emptyset 100mm \times 200mm$	28-day curing in water tank

2.4. *Microstructural analysis*

Broken pieces from 7-day and 28-day mechanical testings were collected and immersed in a 99% isopropanol solution for 24 h to stop the cement hydration. After that, all

to mass loss of all groups at a temperature up to 1000 °C with a heating rate of 10 °C/min. Approximate 30 mg powder of each group was placed in an alumina crucible. A 20-min standby was employed after placing the crucible

in the nitrogen-environment chamber. Based on previous studies [33–35], The nitrogen flow rate was as 50 ml/min for all groups. TG and derivative TG (DTG) curves were plotted for the decomposition analysis of the hydration products at two curing period.

XRD spectra was detected using a Bruker D8 Discover diffractometer (Cu Kα, $\lambda = 1.54$ Å). The measurement process was set at a scanning step of 0.02° from 5° to 70° 2θ. The phase assemblage of the specimens with and without biochar was identified using Crystallography Open Database.

2.5. Chloride-ion resistance test

After 28-day of water exposure, three $\emptyset 100mm$ disks of each group were cut in the middle to achieve a total thickness of 50 mm using a Struers Labotom-15 cutting machine. Each 50-mm disk was then placed in a vacuum desiccator for 3 h. After adding deionized water to fully immerse samples, another 1-hour vacuum curing was employed. After that, samples were immersed in deionized water at least 18 h to remain in saturated status prior to the formal testing. In addition, laboratory-grade sodium chloride and sodium hydroxide pellet (Rowi Scientific, Australia) were added in deionized water to prepare the solutions.

2.5.1. Rapid chloride penetration test (RCPT)

To examine the biochar-cement mortar's resistance against chloride-ion penetration, RCPT test was utilized as per ASTM C1202-22 [36]. Based on a previous study [37], anode reservoir was filled with 0.3 M NaOH solution, and the cathode reservoir was filled with 3 wt % NaCl solution. RCPT was conducted in a testing period of 6 h at working voltage of 60 V. In each group, 3 50-mm samples were tested and the final passed charge was average of three coulomb readings.

2.5.2. NT Build 492

The chloride migration test (CMT) was performed complying with Nordtest NT Build 492 [38]. 10 wt% NaCl solution was prepared using water as the catholyte solution, and 0.3 M NaOH solution was prepared using deionized water as the anolyte solution. After applying initial voltage of 30 V, the new initial potential was adjusted based on initial current values. CMT was continued up to 24 h. Then, samples were axially split into two parts, followed by 0.1 M $AgNO_3$ spray. The CMT coefficient calculations were processed in accordance with details in NT Build 192 calculation process [38]. In should be noted that the final migration coefficients were the average value of three samples.

2.6. Electrical resistivity

A two-probe method was employed to analyze potential effects of the presence of biochar on the electrical resistivity of the biochar-cement composites [39,40]. As shown in Figure 3a, 2 copper net electrodes were placed 20 mm from each end of the cementitious composites during casting. After 28 days of water immersion, samples were dried in the ambient for one hour, ensuring that the surface of each sample was dried. Then, the sample was attached to a Solartron SI 1260 Impedance analyzer *via* two electrodes. In this study, the impedance spectra were recorded using Zplot software with the charged frequency of 1 to 10 MHz. The impedance testing results were interpreted using Zview software.

3. Results

3.1. Hydration kinetics

Hydration evolutions of different samples were presented in Figure 4, including normalized heat flow (Figure 4a) and normalized heat (Figure 4b). The hydration kinetic results were interpreted as per gram of the binder system. It should be noted that the presence of 5 wt% led to a slight reduction in the LC3- cement hydration by approximate one hour when compared to the control group in black line (Figure 4a). However, 10 wt% biochar did not shift the first hydration peak, remaining similar hydration peak than CLC group.

At the first hydration peak up to10 hours, WSB5 group in green line exhibited comparable hydration heat flow when compared to CLC group, where a slight heat reduction was observed from in the timeframe of 8 h to 10 h. WB5 (blue line) had lowest heat flow among samples with 5 wt% biochar. One interpretation could be that waste wood biochar exhibited high water retention then other two biochar. Based on the particle size distribution in Figure 2, WB powders had more coarse grains, reducing the hydration heat due to low reactivity. In terms of

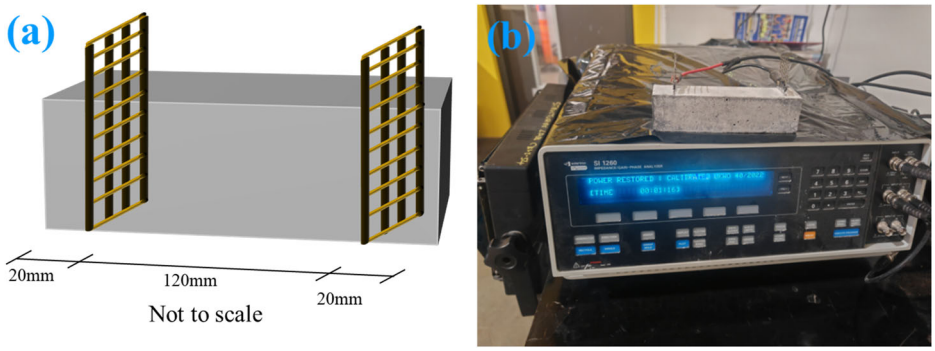

Figure 3. Electrical resistivity test set up: (a) a typical CLC sample with two electrodes; (b) circuit of electrical resistivity test.

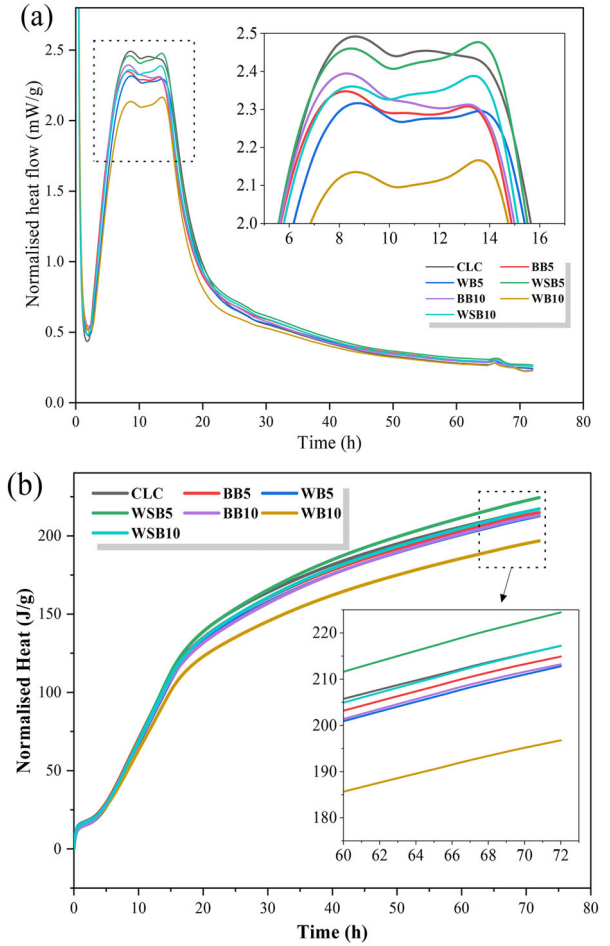

Figure 4. Hydration kinetics of samples with and without biochar: (a) normalized heat flow; (b) normalized heat.

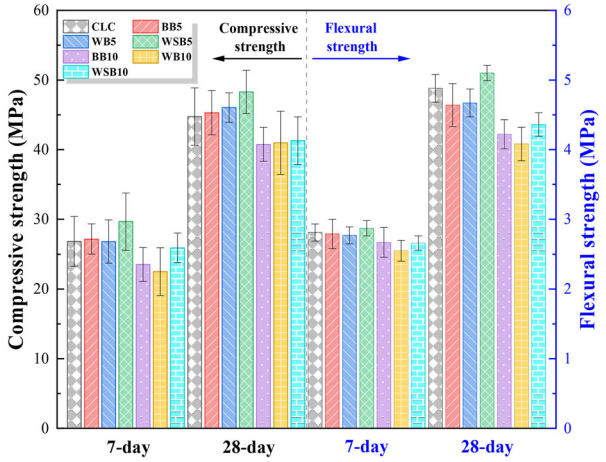

Figure 5. Mechanical properties of samples with and without biochar.

10 wt% biochar as cement replacement, due to the cement dilution effect, heat flow reductions were observed for samples with 10 wt% biochar, having a good agreement with other studies [22,41]. In particular, a heat flow reduction of 3.5 mW/g was found at approximate 8.5 h of the hydration for WB10 group when compared to CLC group. As shown in Figure 2, waste wood biochar had relatively large particles with D90 value of 79.43 μm, large-size pulverized biochar powder would inevitably interfere the hydration process of the cementitious system. A similar observation was reported by Dixit et al. [42], they noted that due to coarser biochar grains, a decrease in hydration flow was found. However, unlike the CLC group experienced gradual flow reduction from 12 h to 15 h, additional hydration flow peak was observed for samples with biochar powder at the hydration timeframe between 13.5 h and 15 h (Figure 4a). Similar observation was reported in a study by Lin et al. [43], due to absorbed water release at early age, biochar could be considered as internal curing agent in cementitious composites. Furthermore, as discussed in other studies [17,44,45], biochar particles released adsorbed water promoting the early-stage hydration. Heat flow at 14.5 h hydration of WSB group was 0.7 mW/g higher than the reference group, where other samples had lower heat flow at this particular period. Due to fine particles of WSB (less than 70 μm), more hydration nucleation sites were offered, contributing to refine the pore structure of the biochar-cement composites and promoting the hydration process. Several studies [43,46] agreed that cement hydration was improved by reducing the particle size of biochar powder, providing both better filler effect and more nucleation sites. However, due to excessive biochar content, samples with 10 wt% biochar still had lower heat flow with additional hydration peak.

As depicted in Figure 4b, WSB group had the highest normalized hydration heat (224.45 J/g) after 72 h of hydration, being 3.34% higher that of the reference group (216.10 J/g). The improved hydration kinetics reflected that finer-size WSB particles had a more favorable benefit assisting the development of hydration products by providing more nucleation sizes. WB5 group (214.89 J/g) and BB5 group (213.76 J/g) demonstrated comparable hydration heat than CLC group. In terms of 10 wt% cement replacement, heat reduction was found in WB10 group (196.76 J/g), being 9.41% less than that of the control group.

3.2. *Mechanical properties*

The mechanical strengths of LC3-cement mortars with and without biochar up to 28-day water immersion were depicted in Figure 5. Mechanical properties were calculated as the average of three specimens for all groups. After 7-day exposure in water, CLC sample had 7-day and 28-day compressive strength of 26.84 and 44.74 MPa respectively with the water to binder ratio of 0.5. Due to relative finer biochar particles (WSB size $\leq$ 70 μm), WSB particles provide proper filler effects improving the cement hydration (Figure 4a), leading to strength increases for 7-day (10.56%) and 28-day compressive strength (7.93%). As shown in Figure 6a, BB5 group (BB size $\leq$ 104.7 μm) and WB5 group (WB size $\leq$ 239.88 μm) remained similar compressive strengths than the control group at 7 days (−0.2% − 2.29%) and 28 days (1.25% − 2.93%). This noticeable difference was attributed to the differences in the pulverized biochar. Coarser biochar particle would interfere with the development of hydration products, leading to a porous microstructure lowering the

strength. Similar observations were reported in several studies [47–49]. Lin et al. [17] summarized that finer-size pulverized biochar powder provide two benefits in the compressive strength development of the biochar-cement composites, including appropriate filler effects and improved cement hydration leading to a denser microstructure and refined microstructure. However, Dixit et al. [50] reported that 5 wt% wood biochar reduced the 28-day compressive strength of ultra-high-performance mortars (UHPC) by 12.5%. This significant difference highlighted that although biochar could provide a denser microstructure of the normal biochar-cement composite, the presence of biochar led to relatively weak area in the UHPC matrix, reducing the 28-day compressive strength of UHPC. In terms of 10 wt% biochar as the cement replacement, lower compressive strengths at both water exposure periods were observed regardless of the type of biochar when compared to CLC group, being −3.47% to −16.21% and −7.72% to −12.61% for 7-day and 28-day compressive strength respectively. Furthermore, it was worth noting that coarser WB particles led to the highest compressive strength reduction of samples with biochar. Similar observation was noted in the study by Asadi et al. [51]. They reported that cement dilution effect contributed to compressive strength decrease of specimens with biochar content above 5 wt%.

However, unlike effects of biochar on the compressive strength development, biochar addition led to flexural strength reduction of the biochar-cement composites (Figures 5 and 6b). For 5 wt% cement replacement, WSB5 group slightly increased the 7-day and 28-day flexural strength by 2.14% and 4.53% respectively. However, 0.71% − 1.42% and 4.25% to 5.02% decrease were found for 7-day and 28-day flexural strength respectively in other two groups with 5 wt% biochar. Furthermore, lower flexural strength was observed in samples with 10 wt% biochar, being 4.98% to 9.25% and 10.74% to 16.47% for 7-day and 28-day flexural strength respectively. Excessive biochar content could lead to a more porous cementitious matrix, negatively interfering with flexural strength development. One interpretation was the unlike compressive forces tend to close pores when loading, flexural forces break the pores prior to damage the denser cementitious matrix. Several studies [52–54] mentioned that high biochar (up to 10 wt%) resulted in more porous areas in the cementitious matrix, reducing the resistance against to flexural loads. Boumaaza et al. [55] added that another factor lowering the flexural strength of the biochar-cement composites was the uneven biochar distribution, where biochar cumulation inevitably created weak plane leading to reduction of the flexural strength. The assemblage of hydration products was analyzed using XRD and TG in the following section.

Overall, by combining the heat evolution (Figure 4) and strength development (Figure 5) of samples with and without biochar, finer-size wheat straw biochar seemed to be more effective in improving both the growth of the cement hydration and strength development of the biochar-cement mortars. The favorable outputs are governed by two aspects: finer-size biochar particles effectively promote cement hydration by offering more nucleation sizes. Secondly, finer-size biochar powder has better filler effects than that of coarser biochar powders. Thus, it could conservatively conclude that although slight reduction is observed at 28-day flexural strength of WSB group, up to 10 wt% finer-size biochar (size $\leq$ 70 μm) could be safely considered as a favorable alternative for designing sustainable cementitious composites, by combining potential economic contributions.

3.3. *Microstructural analysis*

3.3.1. *SEM-EDS*

SEM-EDS analysis was carried out to investigate the biochar-cement matrix. As presented in Figure 7, a WSB particle well embedded in the cementitious matrix, and formation of portlandite and C-S-H gel could be identified. It is worth mentioning that denser cementitious matrix was observed around the biochar particle without the presence of micro-cracks and pores. The reason is that during the early-stage hydration, biochar adsorbs water resulting in relatively low water-to-binder ratio in local region, improving its corresponding density. Similar conclusion was made by a study by Boumaaza et al. [55].

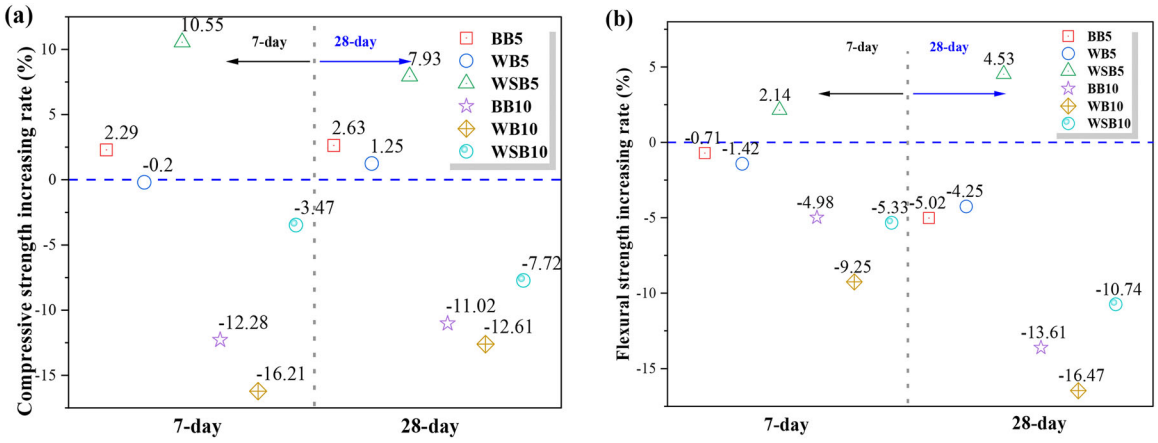

Figure 6. Increasing rate of mechanical strengths at two exposure periods: (a) compressive strength; (b) flexural strength.

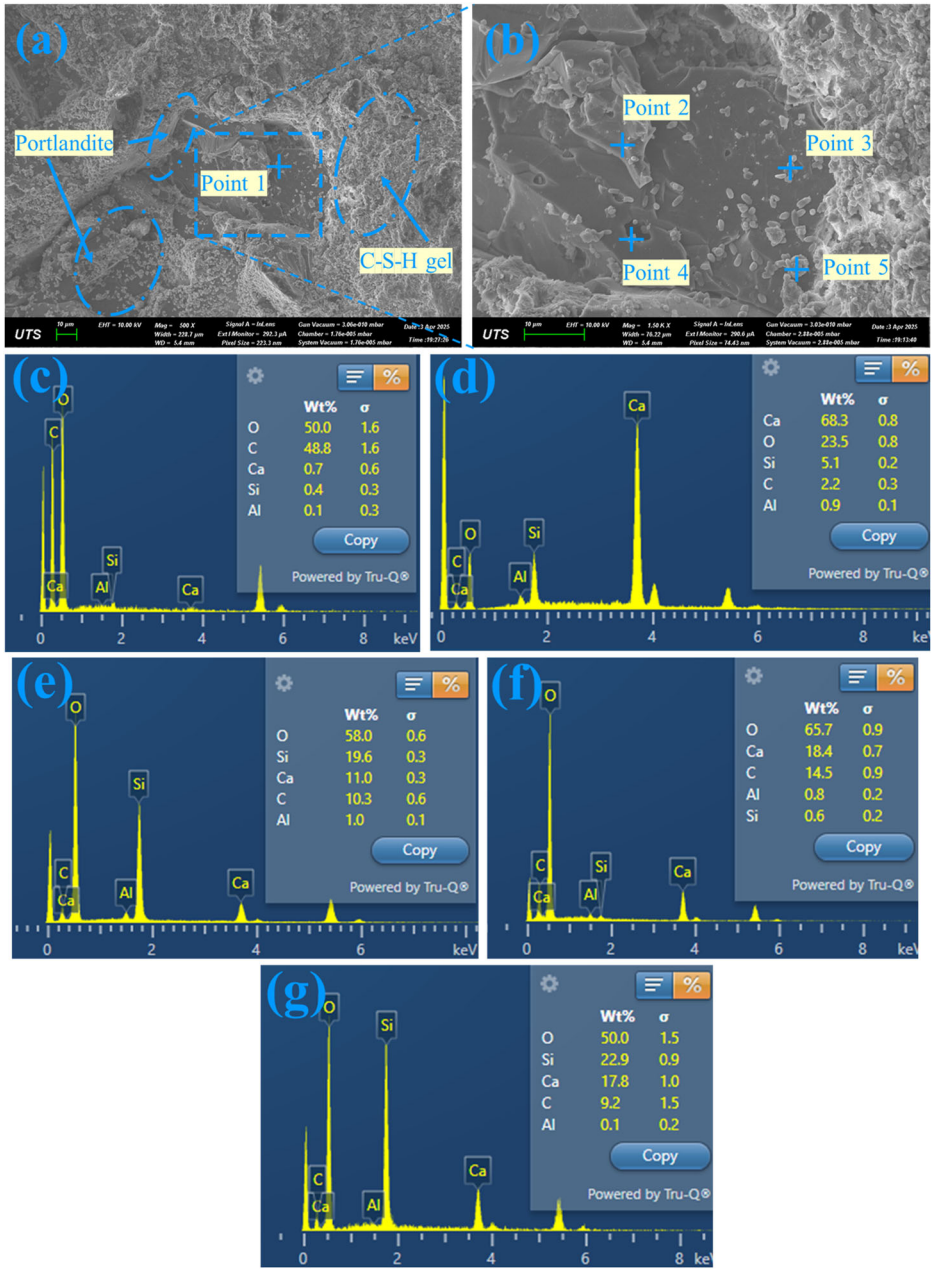

Figure 7. SEM-EDS analyze of a WSB5 sample: (a) WSB in the cementitious matrix; (b) hydration on the surface and pores of a WSB; (c) EDS result of WSB particle in point 1; (d) EDS result of point 2; (e) EDS result of point 3; (f) EDS result of point 4; (g) EDS result of point 5.

EDS result of point scan in point 1 revealed the presence of WSB with high portion of oxygen and carbon. As mentioned by other studies [45,50,55], biochar provided additional hydration sites for the cement hydration, promoting the mechanical strength development. Evidently, formation of portlandite (Figure 7d) and C-S-H gel (Figure 7e and g) were observed on the surface of a WSB biochar particle. Furthermore, it should be noted that formation of calcite was found in the pore of the WSB particle (Figure 7f). This could be due to the carbonation of portlandite in the pore. Figure 8 illustrates additional SEM images of biochar filling in pores of the cementitious matrix, further confirming the favorable characteristics of finer-size biochar densifying the biochar-cement microstructure.

3.3.2. *Phase assemblage*

The phase assemblage development of different LC3-cement mortar with and without biochar at different exposures was depicted in Figure 9. Due to the presence of calcined clay (70 wt% quartz) and siliceous aggregates, the intensity of quartz was relatively higher than other phases (Figure 9a and b), which would not be discussed in this study. 10 wt% limestone contributed to the diffraction peak of calcite at 29.34°, 43.1°, and 48.4° 2θ. It should be noted that due to the presence of 20 wt% calcined clay, ettringite (9.11°, 10.71°, 16.27°, and 40.58° 2θ) and monocarboaluminate (9.11°, 11.66°, and 25.5° 2θ) were detected in the XRD patterns at both exposure period. The formation of monocarboaluminate (Mc) was a complex reaction between Al^{3+}, calcite, and portlandite. At 28-day

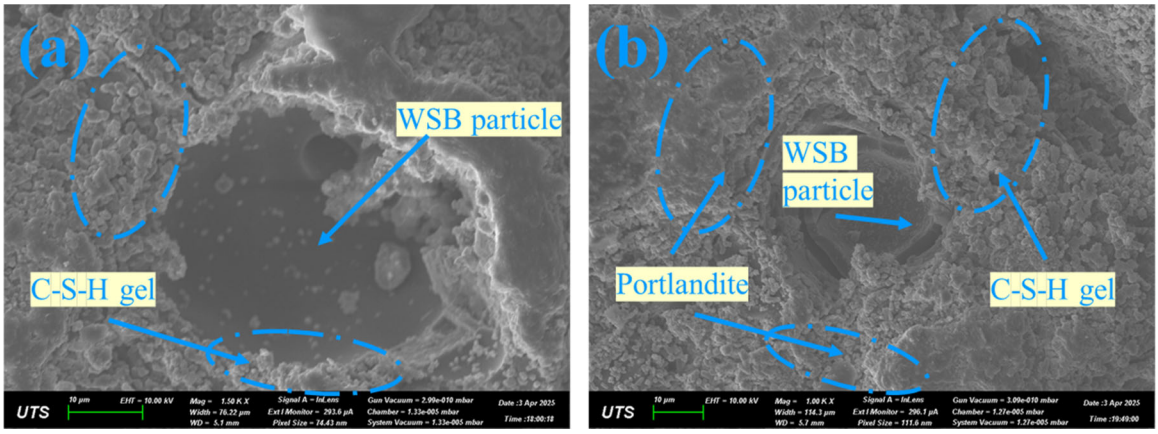

Figure 8. WSB particle filling cementitious pores.

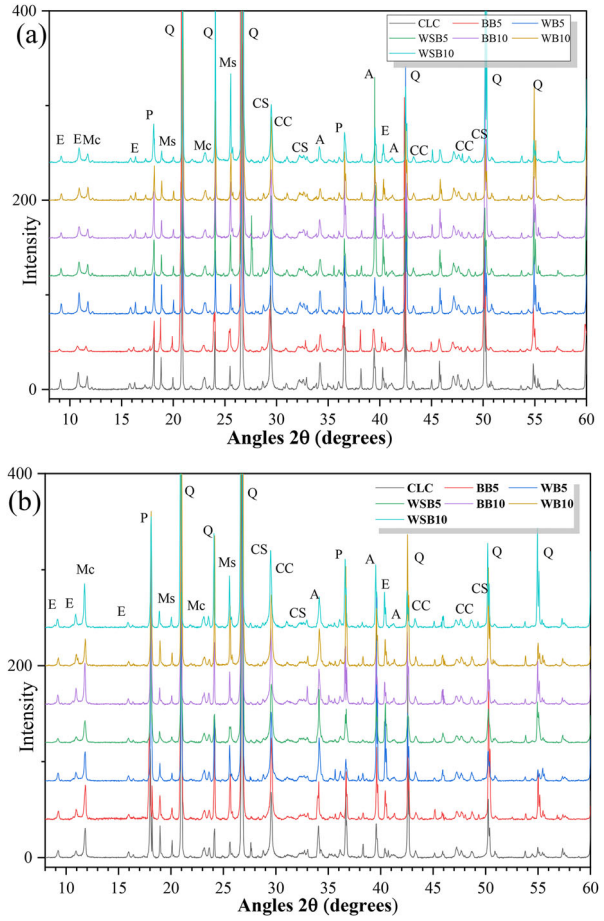

Figure 9. XRD patterns: (a) 7-day water exposure; (b) 28-day water exposure.
(Note: A = Alite (C_3S); CC = Calcite; CS = C-S-H gel; E = Ettringite; Mc = Monocarboaluminate; Ms = Monosulfoaluminate; P = Portlandite; Q = Quartz

water exposure, the intensity of Mc increased, indicating the positive development of chloride-binding capacity of LC3-cement composites. However, based on other studies [56,57], excessive formations of Mc would negatively affect the strength development of the cementitious composites. As shown in Figure 8b, the diffraction peak of Mc in WSB5 sample was lower than other groups, being in a good agreement with the strength development discussion in Section 3.2. Furthermore, by comparing the intensity of ettringite, there was no significant increase in Figure 9b, highlighting the stability of ettringite in the cementitious matrix. A similar conclusion was drawn by Karkhaneh et al. [58]

With the exposure time increased, the diffraction peaks of portlandite (18.02° and 34.11° 2θ) and C-S-H gel (29.33°, 32.3° and 49.7° 2θ) [34] were increased (Figure 9b). Considering the effects of biochar, at 28-day water exposure (Figure 9b), WSB5 group had higher intensity of portlandite peak at 34.11° 2θ, indicating potential improvement of portlandite formation. However, although the diffraction peaks of alite reduced when the curing age increased, it still could be found at 28-day of water exposure (Figure 9b), indicating unhydrated cement grains. The detailed mass changes of the hydration products were calculated using TG/DTG analysis in the following section.

3.3.3. TG/DTG analysis

The TG/DTG results of all groups up to 28-day water exposure were given in Figure 10. Based on the DTG curve (Figure 10a and b), four distinct endothermic peaks were observed. Four thermal events could be interpreted as dehydration of C-S-H gel and ettringite (60 to 150 °C) [33,59,60], decomposition of Mc (150 to 180 °C) [56], decomposition of portlandite (400 to 500 °C), and decarbonation of calcite (600 to 800 °C). It was worth mentioning that since 10 wt% limestone was used to partially replace cement for all groups, the fourth endothermic peak of calcite decomposition was not discussed. Furthermore, some studies [33,59] pointed that no certain verified technique could separate the mass loss of C-S-H gel and ettringite in the temperature up to 150 °C. Thus, this study would only investigate mass loss of bound water (up to 500 °C) and portlandite (400 to 500 °C) using Eq.1 [60] and Equation 2 [61].

$$\delta_{water}\% = M_{60} - M_{500} \quad (1)$$

$$\delta_{CH}\% = (M_{400} - M_{500}) \times \frac{74}{18} \quad (2)$$

where M_{60}, M_{400}, and M_{500} refer to the mass loss percentage in corresponding temperature in TG results. 78 and 18

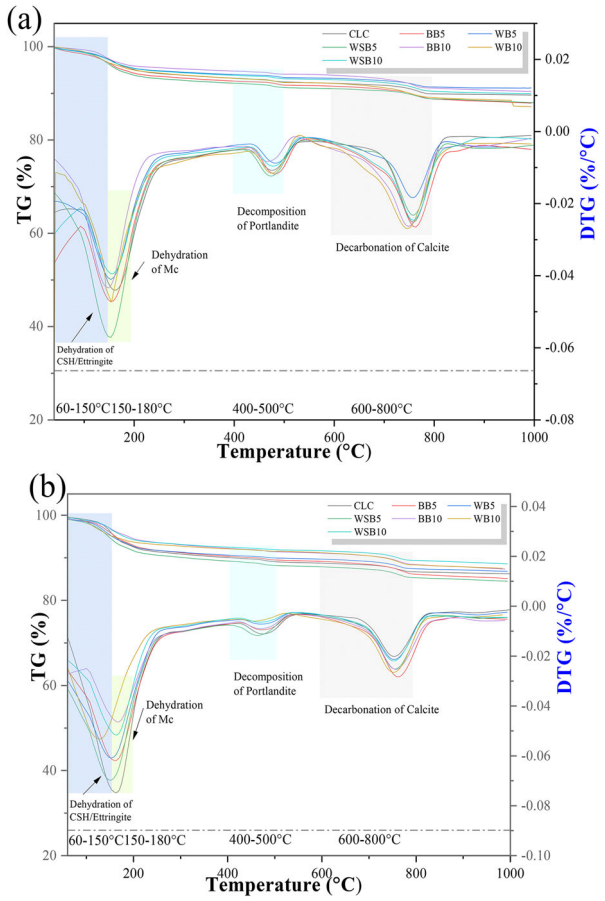

Figure 10. TG/DTG Analysis: (a) 7-day exposure; (b) 28-day exposure.

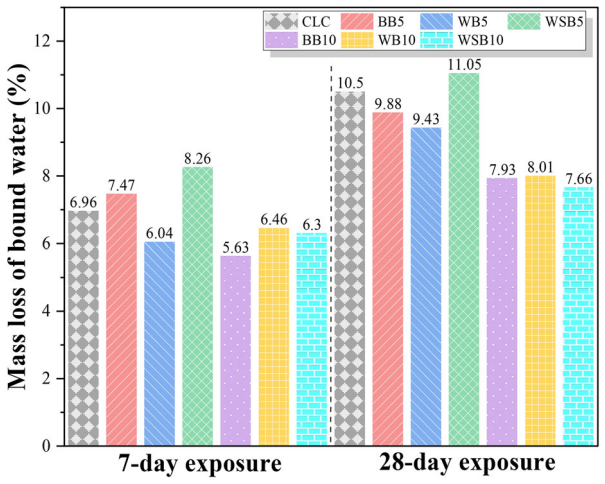

Figure 11. Quantitative analysis of bound water up to 28 days.

represents the molar mass of portlandite and water respectively.

Figure 11 depicts the mass loss of bound water (for all samples up to 500 °C, reflecting the absorbed water for the cement hydration [60]. After a 7-day water immersion, WSB5 samples had the highest δ_{water} of 8.26%, being 18.68% higher than that of the control group (6.96%). BB group exhibited a similar mass loss of bound water than CLC group, and other samples with biochar had lower mass loss of bound water when compared to the reference group. In terms of 28-day exposure, only 5.24% increase in δ_{water} value was found for WSB5 than CLC group. One possible reason is that, although addition of fine-size WSB powder promotes the early-stage hydration (e.g. up to 7-day), 5 wt% cement replacement lowers the hydration degree due to the cement dilution. As depicted in Figure 9b, WSB5 had relatively higher peaks of portlandite, indicating higher degree of hydration than that of the reference group. This phenomenon was more distinct when analyzing samples with 10 wt% biochar. The δ_{water} value for BB10, WB10, and WSB10 was 7.93%, 8.01% and 7.66% respectively, indicating low degree of the cement hydration when compared to biochar-free mortar (10.5%). The investigation of bound water mass loss had a good agreement with hydration analysis (Figure 4) and strength development analysis (Figures 5 and 6) in the previous section.

Based on Equation 2, the effects of various biochar on portlandite mass loss (δ_{CH}) of mortars with and without biochar addition was calculated in Figure 12. Apparently, the content of portlandite increased slightly when the exposure age increased. It should be noted that WSB5 had highest δ_{CH} value of 4.05% and 4.66% for 7-day and 28-day exposure respectively, revealing the favorable characteristic of fine-size biochar (size $\leq$ 70 μm) in improving the cement hydration. In terms of coarser size biochar, the content of BB5 and WB5 was slightly increased, but their portlandite contents were lower than that of CLC group at 28 days. While adding 10 wt% biochar, the formation of portlandite was negatively affected, which would be due to less availability of calcite ions.

Overall, TG/DTG results revealed that finer-size biochar provided surpassing performance than other biochar in promoting the formation of hydration products. Even adding 5 wt% of pulverized WSB biochar with size up to 70 μm, higher mass loss bound water and portlandite was observed (Figures 11 and 12), while coarser biochar exhibited a similar hydration degree with the control group.

3.4. *Chloride resistance*

Chloride resistance of the cementitious mortars could be indirectly represented using RCPT and chloride migration test (CMT) in short term [37,62]. Figure 13 presents experimental results of RCPT and CMT of all groups with water to binder ratio of 0.5, where each value was the average of three identical tests. In terms of RCPT test, samples with 5 wt% biochar addition, had lower passing charges than that of CLC group (1715.83 Coulombs). Gomes et al. [62] added that a denser cement microstructure was more favorable in resisting ion penetrations due to less open accessing channels. WSB5 group reduced the charge by 15.19%, followed by BB5 group with 9.42% reduction on the passing charge. However, WB5 had a close RCPT result (1607.75 Coulombs) with the CLC group. The different performance would be governed by two factors: firstly, fine WSB powder promoted the cement hydration for a denser microstructure, exhibiting the best performance against the passing charges.

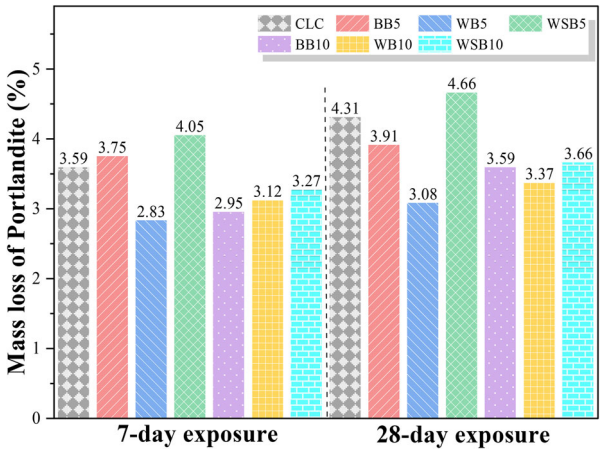

Figure 12. Quantitative analysis of portlandite in different mortars.

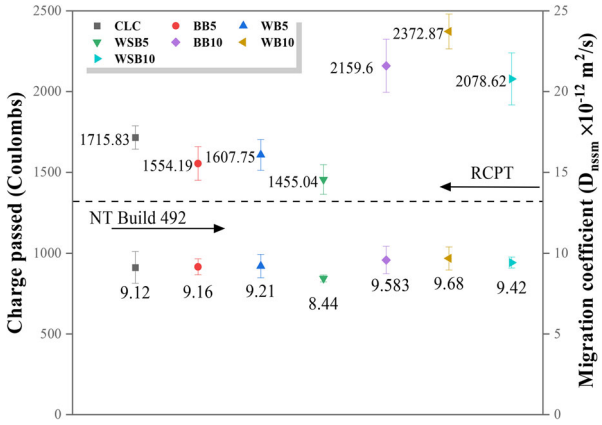

Figure 13. RCPT and chloride migration test results.

Secondly, WSB particle also filled in pores in the cementitious matrix (Figure 8), refining the pore structure to limit the access of the chloride ions. Nguyen et al. [63] agreed that pore refinement could be attributed to lower passing charge in RCPT test. For 10 wt% biochar addition, relatively poor performances of the biochar-cement mortars were found, increasing the charge passed by 21.14% – 38.29%. It should be noted that excessive biochar would not only result in porous cementitious microstructure due to its porous structure but also interfere with the cement hydration resulting in a relative loose biochar-cement microstructure. As a result, more ions could penetrate into the cementitious matrix, lowering the chloride-ion resistance of the samples.

Unlike chloride resistance in RCPT test, BB5 group and WB5 group had slightly large non-steady-state migration coefficient (D_{nssm}) than that of the CLC group. However, WSB5 with the lowest penetration depth of 16.24 ± 0.71 mm (Table 4) still exhibited a favorable resistance of D_{nssm} of 8.44 $\times 10^{-12}$ m^2/s, being 7.45% lower than the control group. As shown Tabel 4, samples with 10 wt% biochar (Figure 14e–g) experienced large penetration depth being 18.61 ± 0.28 mm (BB10), 18.89 ± 0.62 mm (WB10), and 18.15 ± 0.51(WSB) than the reference group (Figure 14a), indicating poor resistance against chloride ion penetration.

Table 4. Mean chloride ion penetration depth in CMT.

Mix design	Depth (mm)
CLC	16.67 ± 0.25
BB5	16.85 ± 0.65
WB5	16.83 ± 0.54
WSB5	16.24 ± 0.71
BB10	18.61 ± 0.28
WB10	18.89 ± 0.62
WSB10	18.15 ± 0.51

Combining the chloride-ion penetration depths (Table 4 and Figure 14) and CMT result (Figure 13), due to porous nature of biochar, only finer-size biochar had improved resistance against chloride ions during CMT test. It worthing noting that slightly different performances of chloride resistance in BB5 and WB5 group were observed in RCPT and CMT. The primary reason may be that at relatively long charging of 24 h, large BB and WB particles may act as additional channels leading to increased penetration depths. Bulk resistivity test was employed to further discuss the electrical resistivity of the mortars with biochar.

3.5. *Electrical resistivity*

The electrical resistivity of samples was plotted *via* Zplot, where real part was the x-axis, and imaginary part was the y-axis. Based on the literatures [39,64], the x value of a right turning point ($R_{m\text{-}AC}$) in a impedance graph could be interpreted as the corresponding electrical impedance of the tested sample. Based on this interpretation, the matrix resistivity of the biochar-cement composites was marked at the x coordinates of each plot (Figure 15). Apparently, the addition of biochar with different replacement percentages led to the various shifting of $R_{m\text{-}AC}$. It shall be noted that the $R_{m\text{-}AC}$ value of WSB5 was approximately 127480 Ω, indicating the highest resistivity among all groups. Similar to chloride-resistance performance, BB5 (123490 Ω) and WB5 (120500 Ω) exhibited a similar electrical resistivity when compared to the CLC group (122900 Ω). In terms of 10 wt% biochar as the cement replacement, excessive biochar particles served as additional electrolytes, reducing the overall resistivity of the biochar-cement composites. Overall, the electrical resistivity results of all samples presented a good consistency with previous chloride-resistance performances of each sample.

4. Discussions on biochar-cement mortar performance using different types of biochar

Figure 16 compares the performances of samples with and without 5 wt% biochar at 28 days. It should be noted that due to excessive presence of biochar particle in 10 wt% cement replacement, their performances are not included in the discussion.

Take hydration process as the starting point, while CLC group had a total normalized heat of 217.11 J/g, and the bound water of CLC was 10.5% at 28 days.

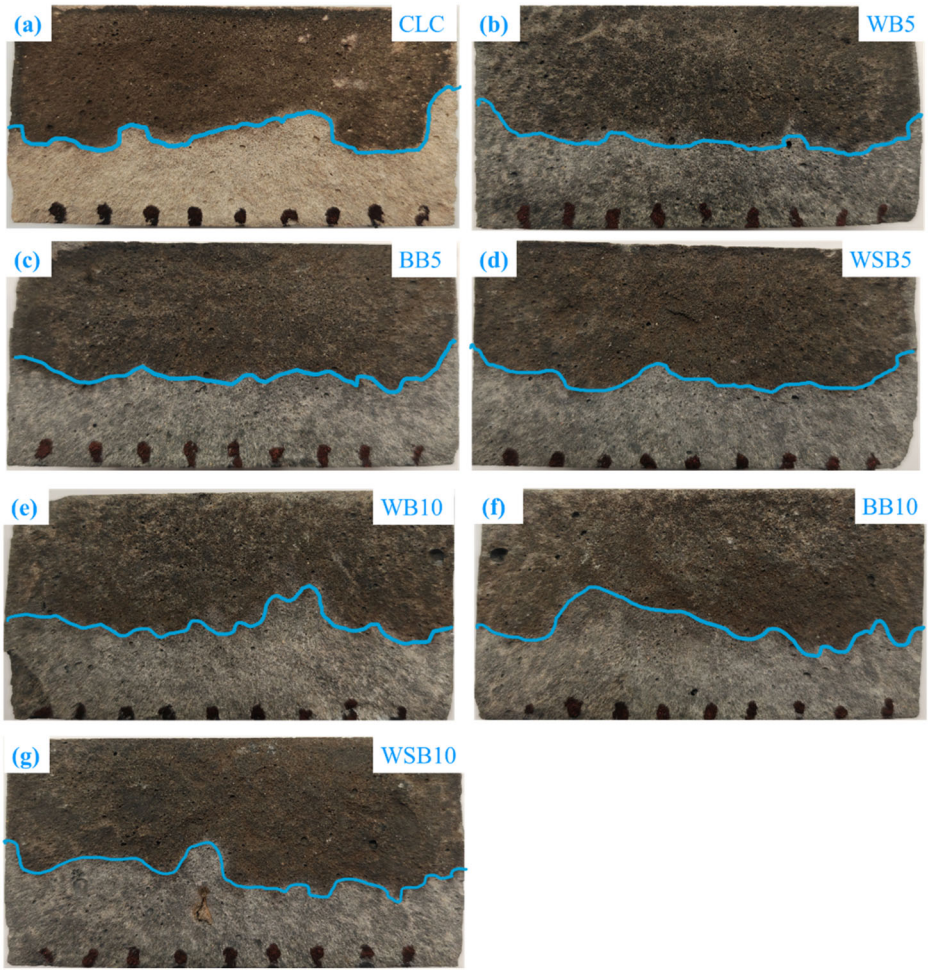

Figure 14. Chloride penetration depth illustrations for all mortars.

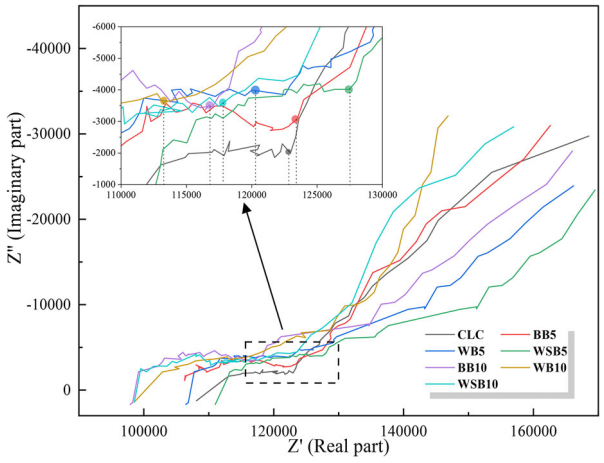

Figure 15. Electrical resistivity of samples with and without biochar using Zplot.

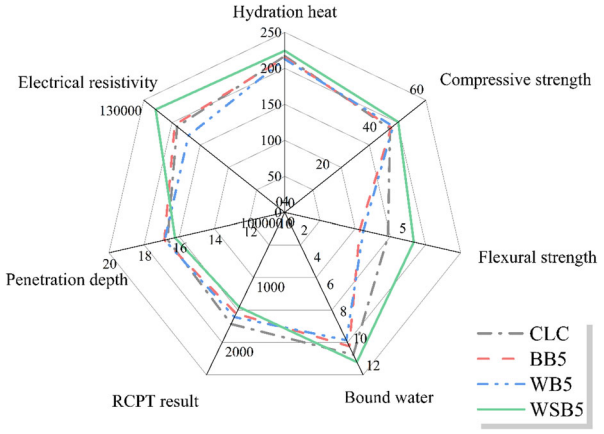

Figure 16. Mortar performance comparisons at 28 days.

Considering this result as the benchmark, WSB5 group surpassed this hydration degree with normalized heat of 224.22 J/g and a bound water mass of 11.05, indicating slightly favorable benefit of finer-size WSB particle in accelerating cement hydration. Based on several studies [65–67], the size of biochar plays a significant role in improving both mechanical and durability properties. The primary mechanism is the filler effect and more nucleation sites for the cement hydration. After comparing the mechanical properties of mortars with various biochar, Lin et al. [17] observed that biochar size $\leq 75\,\mu$m led to more improvement on the compressive strength than samples with coarser biochar.

Evidently, SEM images with EDS scans in Figures 7 and 8 revealed relative compacted formation of the hydration products around the WSB particles. Furthermore, WSB particle also acted as fillers to fill-in the macro-pore of the cementitious composites. As a result, at 28 days, WSB exhibited proper strength increments, e.g. 7.93%

and 4.53% increase in compressive strength and flexural strength respectively. In terms of electrical properties, due to improved hydration kinetics forming more hydration products, a denser WSB-cement matrix demonstrated better chloride resistance and electrical resistivity. On the contrary, due to relatively larger particle size (Figure 2), the hydration process of BB and WB composites was subsequently affected, leading to slightly lower hydration degree (e.g. 214.89 J/g and 212.77 J/g respectively). Consequently, the mechanical and electrical performances were lowered accordingly, having similar performances when compared to the control group.

By comparing the performances of various biochar-cement composites in Figure 16 and available literatures, in this study, 5 wt% finer-size biochar (size $\leq$ 70 µm) could still provide slight improvement on the mechanical properties of the biochar-cement composites, while promoting the durability properties. When the replacement percentage was increased to 10 wt%, both mechanical and durability properties of the sample was negatively affected, having comparable performances with the control group.

Overall, when using various biochar as the SCMs, the most significant factor is the particle size. Up to 10 wt% finer-size wheat straw biochar (size $\leq$ 70 µm) could be safely used to partially replace cement content for designing sustainable cementitious composites. However, only up to 5 wt% biochar is recommended when large biochar particle size is ranging from 70 μm to 239.88 μm.

5. Limitations

Current study focused on potential effects of three biochar on the chloride resistance of LC3-cement composites using RCPT and chloride migration. However, real-world field tests are highly recommended to compare the chloride-binding capacity of biochar-LC3-cement composites. Furthermore, it was found that the biochar particle size had significant impact on the cement hydration process. Thus, it is also suggested that the effects of finer-size or ultrafine-size biochar powder on the hydration and strength development of the biochar-cement composites should be further investigated.

6. Conclusion

Three types of biochar, including commercially available bamboo biochar (BB), and local waste wood biochar (WB) and wheat straw biochar (WSB) was utilized to explore their influences on the hydration, strength development, and chloride resistance of the biochar-cement mortars in this paper. The major findings were drawn as the follows:

1. Due to finer particle size (size $\leq$ 70 µm), WSB5 group exhibited highest hydration heat among all samples, leading to 7.93% improvement on 28-day compressive strength when compared to the reference mortar sample.
2. XRD spectra revealed the increased intensity of C-S-H gel and portlandite, where monocarboaluminate was also detected, which was the complex hydration products of Al^{3+}, calcite, and portlandite.
3. TG/DTG results further verified WSB particle could improve the cement hydration based on higher bound water mass and portlandite mass.
4. Finer-size biochar (WSB) demonstrated better chloride resistance than coarser-size biochar (WB) with low passing charges, less penetration depth, and improved electrical resistance.
5. Up to 10 wt% fine-size wheat straw biochar (size $\leq$ 70 µm) could be safely used as SCMs, having similar strength and durability properties with the control group.
6. The novelty of this study was to comprehensively compare the performances of mortars with various biochar additions, suggesting that 5 wt% coarser biochar (70 μm to 239.88 μm) was the safe dosage as SCMs, while conservative dosage of finer-size wheat straw biochar (size $\leq$ 70 µm) was 10 wt%.
7. Importantly, more studies are required to further clarify the effects of particle size distribution of biochar on other durability properties of the cementitious mortars or concretes, including resistance to carbonation, freeze-thaw cycles, or elevated temperatures.

Disclosure statement

No potential conflict of interest was reported by the author(s).

Funding

The authors highly appreciate Australian Research Council, Australia (DP220101051) and all assistances from University of Technology Sydney Research Academic Program at Tech Lab (UTS RAPT).

ORCID

Quang Dieu Nguyen http://orcid.org/0000-0002-0213-6652
Vivian W.Y. Tam http://orcid.org/0000-0002-1074-8018

Data availability statement

Data will be made available on request.

References

[1] Pillai RG, Gettu R, Santhanam M, et al. Service life and life cycle assessment of reinforced concrete systems with limestone calcined clay cement (LC3). Cem Concr Res. 2019;118:111–119. doi: 10.1016/j.cemconres.2018.11.019.
[2] Imbabi MS, Carrigan C, McKenna S. Trends and developments in green cement and concrete technology. Int J Sustainable Built Environ. 2012;1(2):194–216. doi: 10.1016/j.ijsbe.2013.05.001.

[3] Huang Z, Liang T, Chen L. Experimental studies on durability performances of ultra-lightweight low-carbon LC3 cement composites against chloride ingression and carbonation. Constr Build Mater. 2023;395:132340. doi: 10.1016/j.conbuildmat.2023.132340.
[4] Wang Y, Xu Z, Mi T, et al. Corrosion mechanism of reinforcement in LC3 cement pastes under coupled carbonation and chloride attack. Cem Concr Compos. 2023;140:105080. doi: 10.1016/j.cemconcomp.2023.105080.
[5] McCarthy MJ, Yakub HI, Csetenyi LJ. Impact of fly ash production and sourcing changes on chemical and physical aspects of concrete durability. Constr Build Mater. 2022;342:127313. doi: 10.1016/j.conbuildmat.2022.127313.
[6] Zhou C, Li M, Nguyen QD, et al. Application of waste glass powder for sustainable concrete: design, performance, perspective. Materials. 2025;18(4):734. doi: 10.3390/ma18040734.
[7] Zhan P-M, Zhang X-X, He Z-h, et al. Strength, microstructure and nanomechanical properties of recycled aggregate concrete containing waste glass powder and steel slag powder. J Cleaner Prod. 2022;341:130892. doi: 10.1016/j.jclepro.2022.130892.
[8] Wei H, Wan H, Yuan S, et al. A new gelling material: properties of recycled aggregate concrete under conditions of complete cement replacement using steel slag, ore slag, and fly ash. Constr Build Mater. 2025;464:140180. doi: 10.1016/j.conbuildmat.2025.140180.
[9] Yang B, Han Y, Kong Z, et al. Effect of belite-rich cement on the micro/macro properties and sustainability of slag–oyster powder–cement-based ternary materials. Constr Build Mater. 2025;468:140460. doi: 10.1016/j.conbuildmat.2025.140460.
[10] Gao S, Zhao S, Yang L, et al. Synergistic effects of fly ash-cement slurry and CO2 mineralization on coal gangue aggregate and its concrete properties. Constr Build Mater. 2025;465:140225. doi: 10.1016/j.conbuildmat.2025.140225.
[11] de Klerk D, Naghizadeh A, Ekolu SO, et al. Recycled cement use to produce fly ash – based geopolymer binders suitable for ambient curing: comparison with slag effects. Constr Build Mater. 2025;468:140394. doi: 10.1016/j.conbuildmat.2025.140394.
[12] Pan Q, Peng L, Zhao Y. Mechanisms underlying the long-term reaction in high-volume glass powder cement system. Constr Build Mater. 2025;489:140627. doi: 10.1016/j.conbuildmat.2025.140627.
[13] Li Q, Qiao H, Li A, et al. Performance of waste glass powder as a pozzolanic material in blended cement mortar. Constr Build Mater. 2022;324:126531. doi: 10.1016/j.conbuildmat.2022.126531.
[14] Zhao Y, Zheng Y, Cui K, et al. An innovative ternary carbon-fixing cementitious system of cement-fly ash-carbonated steel slag. Cem Concr Compos. 2025;160:106042. doi: 10.1016/j.cemconcomp.2025.106042.
[15] Pan Z, Zhou J, Jiang X, et al. Investigating the effects of steel slag powder on the properties of self-compacting concrete with recycled aggregates. Constr Build Mater. 2019;200:570–577. doi: 10.1016/j.conbuildmat.2018.12.150.
[16] Li X, Fan Y, Li Q, et al. Experimental study on early-age fracture behavior of cement mortar with the addition of fly ash. Constr Build Mater. 2025;465:140255. doi: 10.1016/j.conbuildmat.2025.140255.
[17] Lin X, Li W, Guo Y, et al. Biochar-cement concrete toward decarbonisation and sustainability for construction: characteristic, performance and perspective. J Cleaner Prod. 2023;419:138219. doi: 10.1016/j.jclepro.2023.138219.
[18] Wang L, Chen L, Tsang DCW, et al. The roles of biochar as green admixture for sediment-based construction products. Cem Concr Compos. 2019;104:103348. doi: 10.1016/j.cemconcomp.2019.103348.
[19] Bhagat TS, Pancharathi RK. Performance, microstructure and carbon sequestration potential of agro biochar based cement mortars. Cem Concr Compos. 2025;156:105867. doi: 10.1016/j.cemconcomp.2024.105867.
[20] Kalderis D, Anastasiou E, Petrakis E, et al. Utilization of biochar from olive tree pruning as additive to cement mortars. J Cleaner Prod. 2024;469:143137. doi: 10.1016/j.jclepro.2024.143137.
[21] Ye P, Guo B, Qin H, et al. Investigation of the properties and sustainability of modified biochar-doped cement-based composite. Cem Concr Compos. 2024;153:105684. doi: 10.1016/j.cemconcomp.2024.105684.
[22] Gupta S, Muthukrishnan S, Kua HW. Comparing influence of inert biochar and silica rich biochar on cement mortar – hydration kinetics and durability under chloride and sulfate environment. Constr Build Mater. 2021;268:121142. doi: 10.1016/j.conbuildmat.2020.121142.
[23] Lin X, Nguyen QD, Castel A, et al. Durability of biochar-cementitious composites incorporating crystalline admixture in chloride and sulphate environments. Constr Build Mater. 2025;458:139554. doi: 10.1016/j.conbuildmat.2024.139554.
[24] Kua HW, Goel A, Teo JHJ. Carbon mineralization, microstructure development and mechanical properties of limestone calcined clay cement enhanced with rice husk ash and biochar (bio-LC3). J Cleaner Prod. 2025;520:146091. doi: 10.1016/j.jclepro.2025.146091.
[25] Chen N, Guo Z, Huang S, et al. Study on the improvement of vegetated concrete substrate by biochar and limestone calcined clay cement. Environ Technol. 2025;46(18):3610–3622. doi: 10.1080/09593330.2025.2473657.
[26] Wang Y-S, Kim T, Lin R-S, et al. Improved high-temperature resistance of limestone calcined clay cement (LC3) paste with biochar: multiscale evaluation and mechanistic analysis. Dev Built Environ. 2024;18:100403. doi: 10.1016/j.dibe.2024.100403.
[27] Wang Y-S, Wang X-Y. Multi-characterizations of the hydration, microstructure, and mechanical properties of a biochar–limestone calcined clay cement (LC3) mixture. J Mater Res Technol. 2023;24:3691–3703. doi: 10.1016/j.jmrt.2023.04.033.
[28] Nguyen QD, Kim T, Castel A. Mitigation of alkali-silica reaction by limestone calcined clay cement (LC3). Cem Concr Res. 2020;137:106176. doi: 10.1016/j.cemconres.2020.106176.
[29] ASTM. ASTM C348-21: standard test method for flexural strength of Hydraulic-Cement mortars. West Conshohocken, Pennsylvania, United States: ASTM International, 2013.
[30] ASTM. ASTM C109-20: standard test method for compressive strength of hydraulic cement mortars. West Conshohocken, Pennsylvania, United States: ASTM International, 2020.
[31] Lin X, Shi T, Nguyen QD, et al. Effects of biochar on hydration, strength degradation, and alkali-silica reaction in sustainable waste glass sand-based mortars. J Build Eng. 2025;114:114316. doi: 10.1016/j.jobe.2025.114316.
[32] Scrivener K, Snellings R, Lothenbach B, et al. A practical guide to microstructural analysis of cementitious materials. Boca Raton, FL: CRC Press; 2016.
[33] Lin X, Nguyen QD, Castel A, et al. Self-healing efficiency of sustainable biochar-cement composites incorporating crystalline admixtures. Constr Build Mater. 2025;458:139542. doi: 10.1016/j.conbuildmat.2024.139542.

[34] Zhan P, Wang J, Zhao H, et al. Impact of synthetic C-S-H seeds on early hydration and pore structure evolution of cement pastes: a study by 1H low-field NMR and path analysis. Cem Concr Res. 2024;175:107376. doi: 10.1016/j.cemconres.2023.107376.
[35] Li P, Li W, Wang K, et al. Hydration of Portland cement with seawater toward concrete sustainability: phase evolution and thermodynamic modelling. Cem Concr Compos. 2023;138:105007. doi: 10.1016/j.cemconcomp.2023.105007.
[36] ASTM. ASTM C1202-22 standard test method for electrical indication of concrete's ability to resist chloride ion penetration. West Conshohocken, Pennsylvania, United States: ASTM International, 2022.
[37] Gomes SDC, Nguyen QD, Li W, et al. Effects of mix composition on the mechanical, physical and durability properties of alkali-activated calcined clay/slag concrete cured under ambient condition. Constr Build Mater. 2024;453:139064. doi: 10.1016/j.conbuildmat.2024.139064.
[38] N.T. Build 492. Concrete, mortar and cement-based repair materials: chloride migration coefficient from non-steady-state migration experiments. Nordtest, Finland; 1999.
[39] Deng Z, Mahmood AH, Dong W, et al. Piezoresistive performance of self-sensing bitumen emulsion-cement mortar with multi-walled carbon nanotubes. Cem Concr Compos. 2024;153:105718. doi: 10.1016/j.cemconcomp.2024.105718.
[40] Hou Y-y, Sun M-Q, Chen J-Z Electrical resistance and capacitance responses of smart ultra-high performance concrete with compressive strain by DC and AC measurements. Constr Build Mater. 2022;327:127007. doi: 10.1016/j.conbuildmat.2022.127007.
[41] Rodier L, Bilba K, Onésippe C, et al. Utilization of bio-chars from sugarcane bagasse pyrolysis in cement-based composites. Ind Crops Prod. 2019;141:111731. doi: 10.1016/j.indcrop.2019.111731.
[42] Dixit A, Verma A, Pang SD. Dual waste utilization in ultra-high performance concrete using biochar and marine clay. Cem Concr Compos. 2021;120:104049. doi: 10.1016/j.cemconcomp.2021.104049.
[43] Lin X, Nguyen QD, Castel A, et al. Effect of biochar on the shrinkage deformation of ground granulated blast-furnace slag-cement mortars. Constr Build Mater. 2026;506:144734. doi: 10.1016/j.conbuildmat.2025.144734.
[44] Zhang J, Wei G, Yang D, et al. Investigation of sludge-based iron-biochar material derived for cement: composites performance, hydration mechanism, and sustainability. Constr Build Mater. 2025;474:141099. doi: 10.1016/j.conbuildmat.2025.141099.
[45] Xiao S, Li Y, Xu C, et al. The influence of biochar addition on the mechanical performance, hydration mechanism, and carbonation capacity of super sulfated cement. Constr Build Mater. 2025;463:140073. doi: 10.1016/j.conbuildmat.2025.140073.
[46] Gupta S, Kua HW, Low CY. Use of biochar as carbon sequestering additive in cement mortar. Cem Concr Compos. 2018;87:110–129. doi: 10.1016/j.cemconcomp.2017.12.009.
[47] Sirico A, Bernardi P, Belletti B, et al. Mechanical characterization of cement-based materials containing biochar from gasification. Constr Build Mater. 2020;246:118490. doi: 10.1016/j.conbuildmat.2020.118490.
[48] Qin Y, Pang X, Tan K, et al. Evaluation of pervious concrete performance with pulverized biochar as cement replacement. Cem Concr Compos. 2021;119:104022. doi: 10.1016/j.cemconcomp.2021.104022.
[49] Haris Javed M, Ali Sikandar M, Ahmad W, et al. Effect of various biochars on physical, mechanical, and microstructural characteristics of cement pastes and mortars. J Build Eng. 2022;57:104850. doi: 10.1016/j.jobe.2022.104850.
[50] Dixit A, Gupta S, Pang SD, et al. Waste valorisation using biochar for cement replacement and internal curing in ultra-high performance concrete. J Cleaner Prod. 2019;238:117876. doi: 10.1016/j.jclepro.2019.117876.
[51] Asadi Zeidabadi Z, Bakhtiari S, Abbaslou H, et al. Synthesis, characterization and evaluation of biochar from agricultural waste biomass for use in building materials. Constr Build Mater. 2018;181:301–308. doi: 10.1016/j.conbuildmat.2018.05.271.
[52] Restuccia L, Ferro GA. Promising low cost carbon-based materials to improve strength and toughness in cement composites. Constr Build Mater. 2016;126:1034–1043. doi: 10.1016/j.conbuildmat.2016.09.101.
[53] Restuccia L, Ferro GA, Suarez-Riera D, et al. Mechanical characterization of different biochar-based cement composites. Proc Struct Integrity. 2020;25:226–233. doi: 10.1016/j.prostr.2020.04.027.
[54] Aneja A, Sharma RL, Singh H. Mechanical and durability properties of biochar concrete. Mater Today: Proc. 2022;65:3724–3730. doi: 10.1016/j.matpr.2022.06.371.
[55] Boumaaza M, Belaadi A, Bourchak M, et al. Comparative study of flexural properties prediction of washingtonia filifera rachis biochar bio-mortar by ANN and RSM models. Constr Build Mater. 2022;318:125985. doi: 10.1016/j.conbuildmat.2021.125985.
[56] Hu S, Liu Q, Cai H, et al. Performance of limestone calcined clay cement (LC3) made with CO2-mineralized concrete slurry waste. J Cleaner Prod. 2024;472:143476. doi: 10.1016/j.jclepro.2024.143476.
[57] Blouch N, Rashid K, Zafar I, et al. Prioritization of low-grade kaolinite and mixed clays for performance evaluation of limestone calcined clay cement (LC3): multi-criteria assessment. Appl Clay Sci. 2023;243:107080. doi: 10.1016/j.clay.2023.107080.
[58] Karkhaneh S, Tarighat A, Ghaffarpour Jahromi S. Kinetics behavior of delayed ettringite in limestone calcined clay cement (LC3) by thermodynamic approach and consideration of the time factor. Constr Build Mater. 2023;367:129143. doi: 10.1016/j.conbuildmat.2022.129143.
[59] Zhang C, Lu R, Li Y, et al. Effect of crystalline admixtures on mechanical, self-healing and transport properties of engineered cementitious composite. Cem Concr Compos. 2021;124:104256. doi: 10.1016/j.cemconcomp.2021.104256.
[60] Zhan P, Xu J, Wang J, et al. Structural supercapacitor electrolytes based on cementitious composites containing recycled steel slag and waste glass powders. Cem Concr Compos. 2023;137:104924. doi: 10.1016/j.cemconcomp.2022.104924.
[61] Zhou F, Pan G, Wang Q, et al. Effects of the surface nano-reconstruction of steel slag on the performance of cement-based materials. Constr Build Mater. 2025;475:141172. doi: 10.1016/j.conbuildmat.2025.141172.
[62] Gomes SDC, Pang Y, Nguyen QD, et al. The effect of calcined clay reactivity on the mechanical properties and chloride diffusion resistance of alkali-activated calcined clay-GGBFS concrete. J Build Eng. 2025;102:111996. doi: 10.1016/j.jobe.2025.111996.
[63] Nguyen QD, Castel A, Kim T, et al. Performance of fly ash concrete with ferronickel slag fine aggregate against alkali-silica reaction and chloride diffusion. Cem Concr Res. 2021;139:106265. doi: 10.1016/j.cemconres.2020.106265.
[64] Berrocal CG, Hornbostel K, Geiker MR, et al. Electrical resistivity measurements in steel fibre reinforced cementitious materials. Cem Concr Compos.

2018;89:216–229. doi: 10.1016/j.cemconcomp.2018.03.015.

[65] Shanmugam V, Sreenivasan SN, Mensah RA, et al. A review on combustion and mechanical behaviour of pyrolysis biochar. Mater Today Commun. 2022;31:103629. doi: 10.1016/j.mtcomm.2022.103629.

[66] Liu J, Liu G, Zhang W, et al. Application potential analysis of biochar as a carbon capture material in cementitious composites: a review. Constr Build Mater. 2022;350:128715. doi: 10.1016/j.conbuildmat.2022.128715.

[67] Yaashikaa PR, Kumar PS, Varjani S, et al. A critical review on the biochar production techniques, characterization, stability and applications for circular bioeconomy. Biotechnol Rep (Amst). 2020;28:e00570. doi: 10.1016/j.btre.2020.e00570.